ATOMIZATION OF SUPERCRITICAL ANTISOLVENT INDUCED SUSPENSIONS – REPLACING ANTI-SOLVENT PRECIPITATORS BY ANTI-SOLVENT NOZZLES

M. A. Rodrigues[1], L. Padrela[1], V. Geraldes[1], J. L. Santos[2], H. A. Matos[1], E. G. Azevedo[1*]
[1] Department of Chemical and Biological Engineering
Instituto Superior Técnico, Av. Rovisco Pais, 1049-001 Lisboa, Portugal
2 Requimte/CQFB, Departamento de Química, Faculdade de Ciências e Tecnologia, Universidade Nova de Lisboa, Campus de Caparica, 2829-516 Caparica, Portugal

Keywords: ASAIS, crystal engineering; supercritical fluids; theophylline; polymorphs; SAS
Topic: Material processing in SCFs

Abstract

Two decades have passed since Gallagher et al. [1] reported a "novel" process to recrystallize compounds insoluble in supercritical fluids – the Gas Anti-Solvent process. Since then the anti-solvent effect has been extensively documented by several authors in its many variations commonly described as GAS and SAS.
In these processes the anti-solvent dissolution and solvent extraction occur in the same unit and causing therefore the competition between two precipitation mechanisms: the supersaturation by solvent extraction and supersaturation by dissolution of the antisolvent, each leading to products with distinct properties.
In this work, we explore a novel approach that consists of separating the dissolution of the antisolvent (CO_2) from the solvent extraction. The antisolvent (CO_2) is mixed in a small mixer immediately before the nozzle in such conditions that cause the precipitation of solutes. The generated suspension is then sprayed for solvent separation by spray drying. This approach permits a better control of the antisolvent process and reduces the volume typical of the high pressure precipitator by several orders of magnitude to a mixer with a few cm^3.
Theophylline (TPL) particles were produced by ASAIS (Atomization of Supercritical Induced Suspensions) from THF (tetrahydrofuran) solutions using antisolvent and non-antisolvent fluids, namely CO_2 and N_2, at various processing conditions (such as *P,T*) . The phase equilibria of theophylline precipitation from THF/CO_2 were studied using a visual cell and the process kinetics studied using Computational Fluid Dynamics.
The results obtained show that particles produced by ASAIS are TPL polymorphs with different properties while particles produced by the same setup at non-antisolvent conditions reveal the common crystal form.
Our results show that by operating within small thermodynamic and kinetic "windows" it is possible to obtain supercritical-antisolvent products by using a specific nozzle setup.

* Corresponding author. Tel + 351-21 841 9394. E-mail: egazevedo@ist.utl.pt

Introduction

During the last two decades Supercritical Anti-Solvent processes have been used to process a myriad of products with applications in multiple fields. Although many authors have been addressing the topic of particle production using supercritical CO_2, as reviewed elsewhere, [2], it is still difficult to point out successful industrial implemented examples. In most cases the main reason halting SAS industrial implementation is the fact that the incremented value of the SAS products is not large enough to balance the costs required for industrial production. It is therefore clear that new strategies for SAS implementation and deeper understanding of the process are required to improve the somewhat cumbersome scale-up of SAS processes.

SAS is usually described as a supersaturation-driven by the exchange of matter between an organic solution and the supercritical fluid, CO_2 in most cases because it is highly miscible with many organic solvents, and it is also supercritical at modest *P,T* conditions as well as non-toxic, and non-flammable and inexpensive. [3] As proposed by Dixon and Johnston [4], mass transfer will dictate whether the precipitation is governed by: (a) anti-solvent crystallization, whenever the solubilization of CO_2 (antisolvent) in the liquid disrupts its ability to solvate the solutes; and (b) crystallization by solvent extraction, if the supersaturation results from the dissolution of the liquid solvent in the supercritical phase. Both mechanisms may also occur simultaneously, leading to the formation of hybrid products. Several authors have addressed this dualism in SAS processes by describing different particle properties depending of the mechanism that originated them. [4-6] Understanding and controlling mass transfer is therefore decisive to control or design the properties of the products.

In this work, we propose a small volume SAS that involves the Atomization of Supercritical Antisolvent Induced Suspensions (ASAIS). In this process, we separate the dissolution of the antisolvent (CO_2) from the solvent extraction. The anti-solvent precipitation occurs in a small volume (of about 1 cm^3) where the solution mixes with the antisolvent generating a suspension. This suspension of crystals is further sprayed into an atmospheric precipitator for solvent separation. Conversely to conventional SAS, the precipitation occurs before the atomization and therefore it is not required spraying into supercritical conditions, which discards the need for high-volume and high-pressure precipitators, because drying occurs by atmospheric spray drying.

Recently, Botin and coworkers [7] have developed a process for the production of particles by SAS in small volumes (the concentric tube antisolvent reactor - CTAR). Without spraying, the CTAR avoids the complicated mass transfer within droplets of multiple sizes (as discussed above) and discards the requirement of high-volume and high-pressure precipitators. Yet, to keep these advantages in scaling up, it would require the multiplication of the capillary tubes — perhaps thousands or millions of times to achieve industrial capacity. Conversely to CTAR, in this work the crystals are not separated by filtration of the suspension, but instead the suspension is sprayed, and therefore the whole anti-solvent process occurs inside the nozzle setup. This feature confers the process a scale-up rationale that is close to a conventional spray drying.

To demonstrate the potential of ASAIS, we studied the production of particles of a theophylline polymorph. The ability of the SCF to induce polymorphism in pharmaceutical drugs has been described by several authors. Many of these polymorphs have also been produced by other techniques, although recently, Subra-Paternault et *al.* [8,9] revealed a new

theophylline polymorph that so far, has only been obtained by SAS with SC-CO_2. We also developed a computational model to simulate the mixing inside the ASAIS mixing chamber. The steady state transport equations for mass, momentum and mass of the solvent were solved with the OpenFOAM CFD software package. The simulations were complemented with phase equilibria studies of theophylline precipitation from THF/CO_2 to understand the precipitation process in transient conditions.
The potential for obtaining unique products with a supercritical setup that is compatible with installed spray drying technology are important advantages of this process regarding the industrial implementation of SAS.

Experimental

Materials

Theophylline (TPL) with a purity of ≥ 99%, mp 545 K, was supplied by BioChemika (USA). THF was obtained from Panreac with a purity of 99.5% (wt.) and was used as received. Carbon dioxide 99.98 % and Nitrogen 99% pure, were supplied by Ar Líquido (Portugal).

Phase Equilibria Studies

The precipitation of TPL from THF solutions was observed in a visual, variable volume high-pressure cell described in detail in a previous work [5]. Five grams of TPL solutions (5 mg/g) in THF were inserted inside the visual cell. The cell was pressurized with CO_2 in small steps, until the formation of a precipitate was observed. To improve accuracy, each plot was repeated at least two times. The liquid phase was stirred (at about 200 rpm) with a magnetic stirrer placed inside the cell.
The THF volume expansion lines were calculated for the binary CO_2/THF using the Peng-Robinson equation of state (EOS) and the Panagiotopoulos-Reid mixing rules. The interaction parameters used in this calculation were obtained from experimental data and published in a previous work. [5]

ASAIS Setup

Figure 1 shows schematically the ASAIS setup. The liquid solution was pumped by a TSP metering pump (model 2396-74) into the ASAIS nozzle where it mixed with a gaseous or supercritical antisolvent. Figure 2 shows a close up with the details of the nozzle. The gas (N_2 or CO_2) was compressed by a Newport Compressor (model 46-13421-2). The nozzle flow was measured by a mass flowmeter (Rheonik, model RHM007) and pressures were measured by transducers (Omega, model PX603). Temperatures were controlled, in the air chamber and in the water bath, by T-type thermocouples and Ero Electronic controllers (model LDS). The particles were collected in the precipitator walls and in a cyclone (Separex). A nozzle with a 150 μm orifice was used in the experiments with N_2, whereas a nozzle of 100 μm orifice was used in the experiments with CO_2. A smaller nozzle orifice was selected for the processing with CO_2 to limit its flow rate and nozzle freezing due to strong depressurizations.

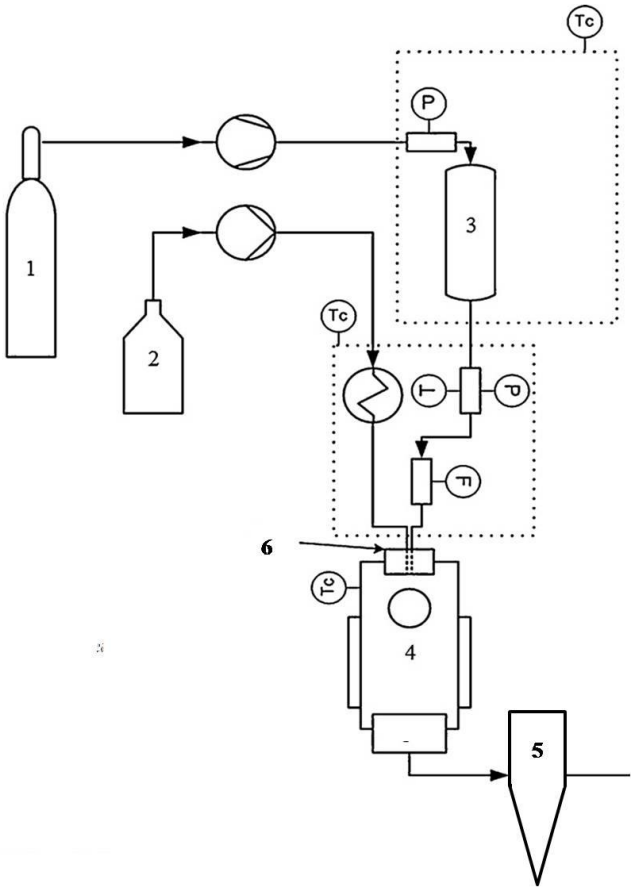

Figure 1 – Schematic representation of the ASAIS experimental setup. (1) CO_2 /N_2 cylinder; (2) liquid solution flask; (3) temperature-controlled CO_2 storage cylinder; (4) precipitator; (5) cyclone; (6) ASAIS nozzle. The nozzle is described in Figure 2 in more detail.

Particles Characterization

The particle morphologies were analyzed by a Scanning Electron Microscope (SEM) Hitachi S2400. Particle samples were coated prior to measurement with a gold film by electrodeposition in vacuum.

Powder X-ray Diffraction (PXRD)

The patterns for different samples were collected on a Bruker D8 Advance powder diffractometer using Cu Kα radiation (1.54056 Å) in a Bragg Brentano geometry. The tube voltage and amperage was 40 kV and 40mA, respectively. The divergence slit and antiscattering slit settings were variable for illumination of the 20 mm sample. Each sample was scanned with 2θ between 5º and 40º with a step size of 0.02º and 0.5 s at each step.

Physical and mathematical model

A longitudinal cross-section of the computational domain of the device where the THF is mixed with the supercritical CO_2 is displayed in Figure 2. The THF inlet tube has a diameter D_1 = 1 mm, and the cell chamber diameter and length are D_2 = 5 mm and L_2 = 25 mm, respectively. An inlet region with a length L_1 = 5 mm was considered in order to obtained developed velocity profiles at the top of the mixing chamber.
Under supercritical conditions, only one fluid phase is present in the device. The objective of the simulation is to predict the distribution of the THF concentration in the mixing chamber in steady-state laminar flow. Due to the difference of physical properties between pure THF and supercritical CO_2, the density, viscosity and diffusivity of the mixture are functions of the THF mass fraction (ω_{A1}). Laminar flow prevails in the whole domain because the inlet velocities are low and the dimensions of the mixing chamber are small. Inside this chamber the pressure is almost constant and the fluid mixture may be assumed incompressible.
For steady state laminar flow of an incompressible Newtonian fluid with a single phase, the transport equations for mass, momentum and mass of the first solute are

$$\nabla \cdot (\rho \mathbf{U}) = 0 \qquad (1)$$

$$\nabla \cdot (\rho \mathbf{U}\mathbf{U}) = \nabla \cdot P + \nabla \cdot (\mu \nabla \mathbf{U}) + \rho \mathbf{g} \qquad (2)$$

$$\nabla \cdot (\rho \mathbf{U} \omega_{A1}) = \nabla \cdot (\rho D_{AB} \nabla \omega_{A1}) \qquad (3)$$

where U is the velocity vector, P is the fluid pressure, ω_{A1} is the mass fraction of THF and **g** is the gravitational acceleration vector. The viscosity (μ), density (ρ) and diffusivity (D_{AB}) were assumed to vary linearly with ω_{A1}. As the difference of density between the THF and the supercritical CO_2 was high, the gravity force was used in the momentum transport equation.
Regarding the boundary conditions, uniform fluid velocity was imposed in the THF and CO_2 inlets and zero gradients for the different variables were imposed in the cell outlet. In the solids walls, the non-slipping condition was used. As the flow was axisymmetric, only 1/4 of the domain was simulated, with recourse to symmetry planes, to reduce the simulation time. The constants used in the simulation are presented in Table 1.

Table 1 – Constants used for the calculations. F refers to the volumetric flow-rate measured experimentally.

F_{THF} m^3/s	F_{CO_2} m^3/s	$D_{THF\text{-}CO2}$ (in liq. THF) [11] m^2/s	$D_{THF\text{-}CO2}$ (in superc.CO2) m^2/s	ρ_{CO_2} [11] kg/m3	ρ_{THF} kg/m3	μ_{CO_2} [11] Pa.s	μ_{THF} Pa.s
8×10^{-7}	3×10^{-8}	3×10^{-8}	5×10^{-9}	400	890	3×10^{-5}	4×10^{-4}

Numerical method

The steady state transport equations for mass, momentum and mass of the first solute were solved with the OpenFOAM CFD software package [10], which is based on the finite-volume formulation with a collocated variable arrangement. Block-structured hexahedral grids were generated using the OpenFOAM blockMesh utility. Parameterization of the computational domain was carried out in order for facilitating the variation of both its dimensions and number of computational cells.
The solver developed in this work used the SIMPLE algorithm for pressure-velocity coupling. The convection terms in the equations were discretized with the upwind scheme. The linear

solvers used here were the geometric agglomerated algebraic multi-grid (GAMG) solver for pressure with 100 cells at the lowest multi-grid level, and the preconditioned bi-conjugate gradient (PBiCG) solver for the remaining variables. The solver relative and absolute tolerances were set, respectively, to 0.01 and 10^{-6} for pressure, and 0.1 and 10^{-5} for velocity and solute. Under-relaxation was used in the steady state solver, with values of 0.3 for pressure and solute, and 0.7 for velocity.
Simulations were processed in parallel on a 236 node AMD Opteron cluster with 2.8 GHz CPU's and 1 GB RAM/CPU. The computational grids were decomposed for parallel processing considering a ratio of 100 thousand cells/CPU. After grid independence tests, a mesh with 100.000 nodes was found adequate to obtain grid-independent results.

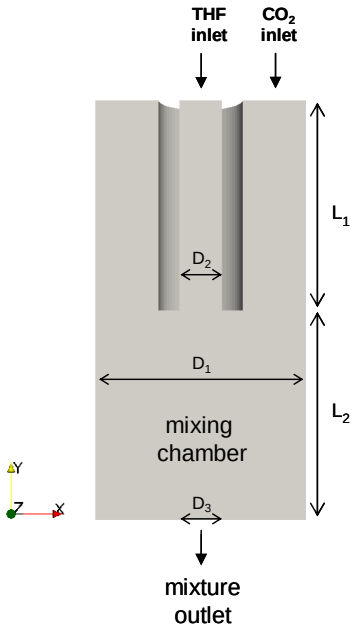

Figure 2 – ASAIS nozzle. Longitudinal cross-section of the computational domain. D_1 = 1 mm, D_2 = 5 mm, L_2 = 25 mm, L_1 = 5 mm.

Results

Precipitation of theophylline by anti-solvent effect

The anti-solvent effect of CO_2 in THF/TPL solutions was observed for several temperatures. An intense nucleation could be observed inside the visual cell when precipitation conditions were reached. At the precipitation conditions (*P,x)* the formation of a "milky" liquid phase was observed, followed by the appearance of small crystals in suspension (after a few minutes). The crosses in the diagram of the Figure 3 show the precipitation points determined experimentally, while the lines were calculated using a model described elsewhere [5].

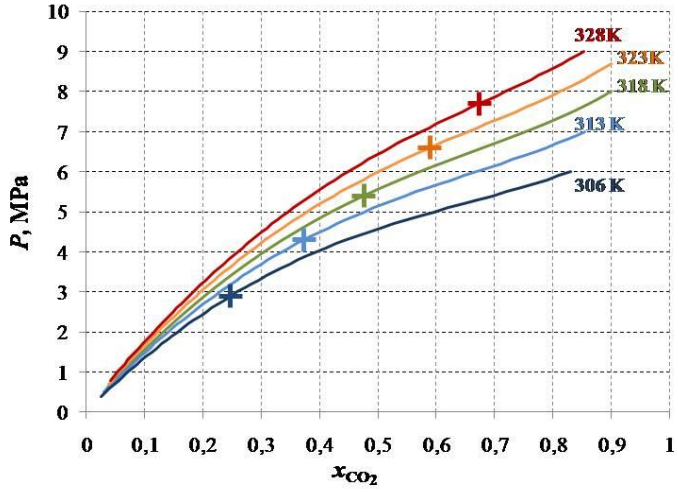

Figure 3 – Precipitation points observed experimentally (crosses) plotted in (P, x_{CO_2}) isoterms calculated with the Peng-Robinson EOS.

The CO_2 composition in the liquid phase (x_{CO_2}) in Figure 3 was calculated assuming that the system is a pseudo-binary (CO_2/THF). Although this is not accurate, because the presence of TPL should shift the equilibrium within an error of a few percent, the pseudo-binary assumption is acceptable for qualitative interpretation, as it is intended in this work. For processing rationale, the crosses in Figure 3 represent the minimum pressure (at constant T) required to assure the precipitation of TPL by the anti-solvent effect of the dissolving CO_2. As temperature increases, TPL precipitates for higher composition of CO_2.

Morphological characterization of theophylline particles

Figure 4 shows SEM images of theophylline particles obtained by ASAIS processing at the various conditions presented in Table 2. The crystals are mostly sub-micronic except for the particles produced at high pressure CO_2 (10 MPa) (image "d"), which are in the range of 1 micron. The particles shown in the images "a" to "c" in Figure 4 were produced at non-anti-solvent conditions, as it can be inferred from Table 2~~1~~, because~~.~~ N_2 has no anti-solvent effect and "b" conditions (with CO_2) are below the precipitation point, described in Figure 3. Image "d" refers to anti-solvent conditions well above the observed onset of TPL nucleation for 318 K.

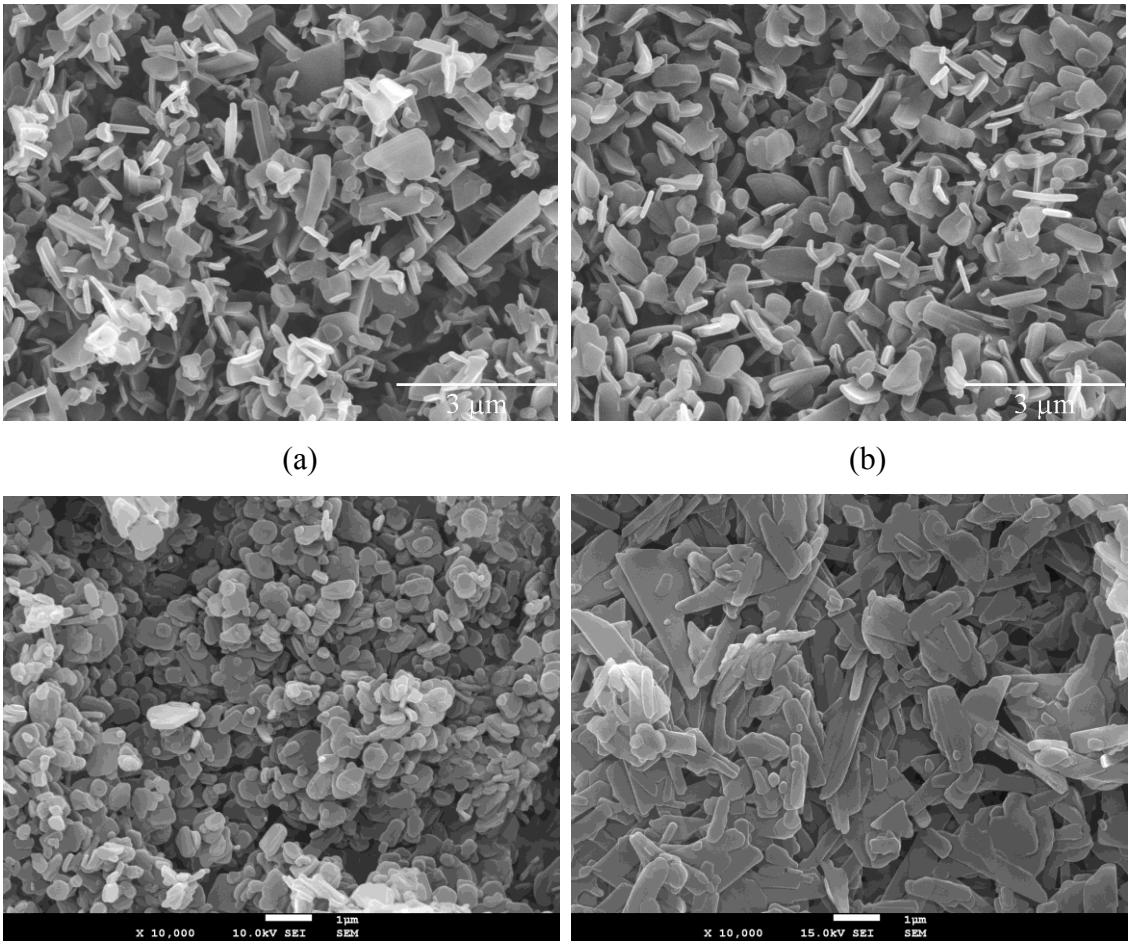

(a) (b)

(c) (d)

Figure 4 – SEM images of particles (10.000 x magnification) produced with N_2 (left) and CO_2 (right). Image (b) refers to non-anti-solvent CO_2 processing, while image (d) refers to anti-solvent CO_2 processing.

Table 2 – Experimental conditions used in ASAIS runs referent to the SEM images shown in Figure 4: *P* (mixing pressure), C_0 (TPL concentration in THF solution), *R* (mass flow-rate ratio of the solution to the supercritical fluid). Temperature was 318 K in all runs.

Image reference	Fluid	*P* MPa	C_0 % mass	*R*
a	N_2	5	0.5	0.21
b	CO_2	5	0.5	0,12
c	N_2	10	0.2	0,11
d	CO_2	10	0.2	0,06

PXRD of theophylline particles

Figure 5 shows PXRD diffractograms obtained for the four samples shown in the images in Figure 4. New diffraction peaks can be observed in Figure 5 for the sample obtained from

high-pressure CO_2 (conditions of image "d"). Yet, using either N_2 or CO_2 below precipitation conditions, the normal crystal form was obtained.

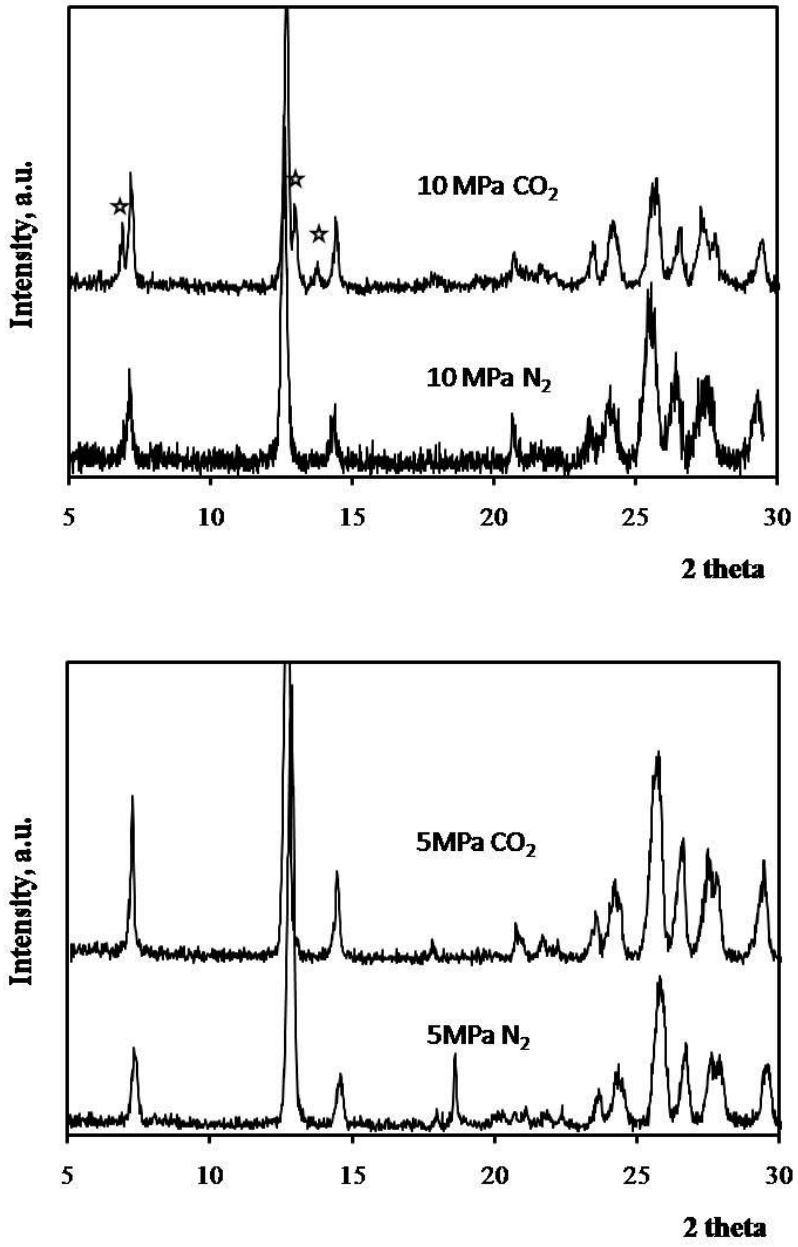

Figure 5 – PXRD diffractograms of the TPL samples shown in Figure 4. The polymorph TPL diffraction peaks are marked with a star.

Composition histogram calculated by CFD

Figure 6 shows the solvent mass composition calculated for the mixing of THF and CO_2 at 10 MPa at 318 K. From Figure 3 we can observe that, at this temperature, it is 0.48 the CO_2 mole fraction required to precipitate TPL, which corresponds to a THF mass fraction (ω_{A1}) of 0.64.

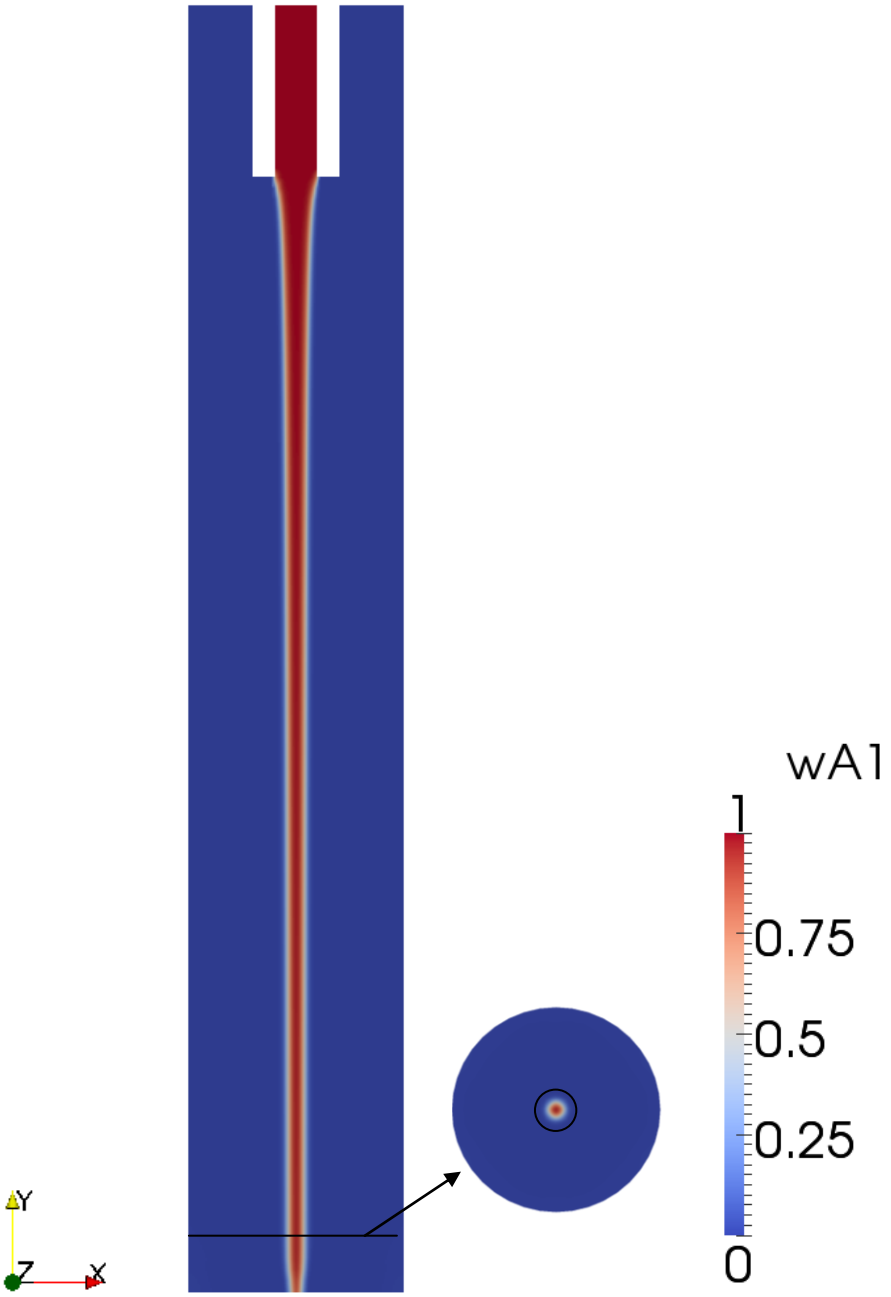

Figure 6 - THF mass fraction (ω_{A1}) inside the mixing chamber predicted by CFD. The radial slice shows the composition close to the nozzle orifice compared to the area of THF at the inlet (represented by a black circle).

Figure 6 shows that the TFL inserted in the mixing chamber mixes almost completely beyond the composition required for TPL precipitation at 318 K (mass fraction of 0.63). In the radial slice (Figure 6) it can be observed a small dark red area (unmixed) compared to the initial area (the black circle).

Discussion

Figure 5 show that TPL particles produced by ASAIS under anti-solvent conditions have a polymorph crystalline structure. The same TPL polymorph has been reported by Subra-

Paternault *et al.* [8] who studied the crystalline phase of TPL processed by SAS and GAS. Until now, this crystalline form was obtained by SC-CO_2 processing only. The same authors showed that the relative intensity of the polymorph peaks increased with pressure, and that the new structure became preponderant as the pressure increased [8]. The polymorph peaks preponderance of the PXRD diffractogram of TPL particles produced by ASAIS (at 10 MPa — see Figure 5) it is very similar to the PXRD pattern obtained by Subra-Paternault *et al*. by SAS for the corresponding conditions. The match between these two cases shows that ASAIS is a small-volume SAS process, as long as the mixing conditions are selected properly.

Two criteria revealed to be fundamental for ASAIS processing. The first is that the conditions must be selected for anti-solvent precipitation to start inside the mixing chamber. Otherwise the particles will only precipitate after atomization by solvent evaporation and no polymorphs will form. As shown in Figure 3, there is a lower limit of pressure required for TPL to precipitate, which is significantly temperature-dependent. If the CO_2 composition in the liquid phase is below the precipitating composition (as shown in Figure 3 for TPL), no influence of anti-solvent effect is observed in the crystalline structure, and therefore the PXRD pattern is equivalent to N_2 processing. i.e. spray drying. Nitrogen never causes anti-solvent precipitation regardless of pressure, because it is little miscible with THF. The second criterion is the residence time. Even though higher chambers would enable better mixing, it would also extend the time for crystal growth. Conversely to SAS, in ASAIS the contact time of the liquid with the antisolvent has to be small. In the SAS there is no imposed limit for crystals to grow inside the precipitator. However, in ASAIS the nozzle orifice dimension is a physical barrier for the larger crystals in suspension. Therefore, a fine balance between fluid mixing and crystallization kinetics must be found. Figure 6 shows that for the selected geometry, both fluids mix almost completely inside the mixing chamber. This correlates well with experiment, because polymorphs did form revealing that anti-solvent precipitation happened but no precipitate was found inside the mixing chamber, meaning that the crystals were small enough to pass the orifice. In fact, Figure 4 shows that the particles are sub-micrometric, i.e. two orders of magnitude smaller than the nozzle orifice (100 μm) and are as a result unlikely to be retained. However, other results (not shown here) revealed that using chambers with a length twice that presented here, large crystals were entrapped inside the mixing chamber. Conversely, smaller chambers (six times smaller) did not produce polymorphs, notwithstanding the high pressure (10 MPa).

Limiting the anti-solvent effect to a specific time, from the inlet until nozzle discharge, enables ASAIS a better control of the particles' size distribution, if compared to SAS. In SAS particles are usually collected in a filter at supercritical conditions and therefore may still grow until the end of the run, since the supercritical media still possesses reminiscent solvent power.

The ASAIS approach should also simplify the particles' collection, because the pressure after the nozzle is close to atmospheric, particles may be recovered using a cyclone, as in conventional spray drying.

Conclusion

The results presented in this work show that SAS can be confined to a small volume nozzle setup. By replacing the SAS high-pressure (typically 10-20 MPa) precipitator for a small (few cm^3) pre-nozzle high-pressure mixing chamber, it is possible to obtain equivalent SAS polymorphs while reducing a few orders of magnitude the high-pressure volume. Moreover,

the anti-solvent effect is limited to the residence time of the mixing chamber, which enables a better control of the crystallization and hence the particles' size distribution.
The near atmospheric pressure precipitator works in ASAIS more like a separator to clarify the particles in suspension from the solvent. This feature confers ASAIS good compatibility with established spray drying industry, since the anti-solvent high-pressure part of the process is confined to a small equipment — the ASAIS nozzle. It is therefore likely that this process may be successfully applicable to the production of novel pharmaceutical polymorphs.

ACKNOWLEDGEMENTS
The authors are grateful for financial support to FCT (Grants SFRH/BD/39836/2007 and PTDC/EQUFTT/099912/2008) and E.U. Program FEDER.

Bibliography

[1] - GALLAGHER, P.M., COFFEY, M.P., KRUKONIS, V.J., KLASUNITS, N. Supercritical Fluid Science and Technology, Johnston, K. P., Penninger, J. M. L., Eds., ACS Symposium Series 406, American Chemical Society, Washington, DC: **1989**, p. 334

[2] – REVERCHON, E., ADAMI, R., CAPUTO, G., DE MARCO, I., TORINO, E., J. of Supercritical Fluids 47 **2008,** p. 70

[3] - CANSELL, F., CHEVALIER, B., DEMOURGUES, A., ETOURNEAU, J., EVEN, C., GARRABOS, Y., PESSEY, V., PETIT, S., TRESSAUD, A., WEILL, F. , J. Mater. Chem. 9, **1999**, p. 67

[4] - DIXON, D. J., JOHNSTON, K. P., J. App. Polym. Sci. 50, **1993**, p. 1929

[5] – JUN, L., RODRIGUES, M. A., PAIVA, A., MATOS, H.A., GOMES AZEVEDO, E., J. Supercritical Fluids, **2007** 41, p. 343

[6] - RODRIGUES, JUN, L., M. A., PADRELA, L., ALMEIDA, A.,J., MATOS, H.A., GOMES AZEVEDO, E., J. Supercritical Fluids, 48 **2009** p. 253

[7] – BOUTIN O., MARUEJOULS, C., CHARBIT G., J. of Supercritical Fluids 40, **2007** p. 443

[8] – SUBRA-PATERNAULT, P., ROY, C.,VEGA-GONZALEZ A., VREL D., Proceedings of the IX ISSF Arcachon, France, 2009

[9] – ROY, C., VEGA-GONZALEZ, A., SUBRA-PATERNAULT, P., International Journal of Pharmaceutics, **2007**, p. 79

[10] - OpenCFD Ltd, OpenFOAM: The Open Source CFD Toolbox. http://www.opencfd.co.uk/openfoam/.

[11] - SILVA, C. M., MACEDO, E. A., Ind. Eng. Chem. Res. **1998**, 37, p. 1490